Towards a fundamental understanding of natural gas hydrates

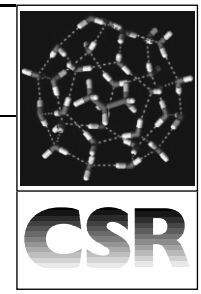

Carolyn A. Koh

King's College London, Department of Chemistry, Strand, London, UK WC2R 2LS. E-mail: carolyn.koh@kcl.ac.uk; Fax: 0207-848-2810; Tel: 0207-848-2380

Received 30th October 2001
First published as an Advance Article on the web 17th April 2002

Gas clathrate hydrates were first identified in 1810 by Sir Humphrey Davy. However, it is believed that other scientists, including Priestley, may have observed their existence before this date. They are solid crystalline inclusion compounds consisting of polyhedral water cavities which enclathrate small gas molecules. Natural gas hydrates are important industrially because the occurrence of these solids in subsea gas pipelines presents high economic loss and ecological risks, as well as potential safety hazards to exploration and transmission personnel. On the other hand, they also have technological importance in separation processes, fuel transportation and storage. They are also a potential fuel resource because natural deposits of predominantly methane hydrate are found in permafrost and continental margins. To progress with understanding and tackling some of the technological challenges relating to natural gas hydrate formation, inhibition and decomposition one needs to develop a fundamental understanding of the molecular mechanisms involved in these processes. This fundamental understanding is also important to the broader field of inclusion chemistry. The present article focuses on the application of a range of physico-chemical techniques and approaches for gaining a fundamental understanding of natural gas hydrate formation, decomposition and inhibition. This article is complementary to other reviews in this field, which have focused more on the applied, engineering and technological aspects of clathrate hydrates.

Carolyn A. Koh was appointed Reader in Chemistry at King's College London in September 1998. She took up a lectureship at King's College in August 1993 after working on spectroscopic and molecular simulation studies of associating fluids at Cornell University. She has been a visiting Professor at Cornell University, USA, a consultant for the Gas Research Institute in Chicago, and is a Fellow of the Royal Society of Chemistry. Since 1994, she has been the Group Leader of a major international project on gas hydrates. Her current research interests cover several aspects of materials chemistry, including fundamentals of gas hydrates, crystal growth processes, and new materials for pollution control. In particular, a major research area she is currently working on is directed towards the molecular mechanisms for the formation, inhibition and promotion of clathrate hydrate systems using spectroscopic, diffraction and molecular modelling methods. This work has led to her recent award of the Young Scientist Award 2001 of the British Association for Crystal Growth.

1 Introduction

1.1 Structural and physico-chemical properties of gas hydrates

Gas hydrates (which are examples within the broader class of clathrate hydrates) were first identified in 1810 by Sir Humphrey Davy[1] and their composition established by Faraday.[2] However, it is believed that other scientists, including Priestley, may have observed their existence before 1810. They are solid crystalline inclusion compounds consisting of a hydrogen-bonded water network of polyhedral water cavities which encage small gas molecules. Many of the components of natural gas form gas hydrates at low temperatures (typically below about 275 to 285 K) and elevated pressure (typically 2.5 to 11 MPa). There are three common types of gas hydrate structure: sI hydrate, sII hydrate, and sH hydrate. The crystal structures of these gas hydrates are illustrated in Figs. 1(a)–(c). These structures differ in the number and sizes of the cages and in their unit cells (see Table 1 and Figs. 1 and 2). The type of crystal structure that forms depends on the size of the guest molecule, *e.g.* CH_4 and C_2H_6 both form sI hydrate, C_3H_8 forms sII hydrate, while larger guest molecules such as cyclopentane in the presence of methane form sH hydrate. Dimethyl ether forms a less common hydrate structure, sT hydrate, which has a much lower small-to-large cage ratio than the other known structures (see Table 1). Both sI and sII hydrates have cubic crystal structures, while sH hydrate has a hexagonal crystal structure and sT hydrate has a trigonal crystal structure (others are currently being identified, see Section 1.2). All these hydrate structures are composed of two or more types of water cages packed within the crystal lattice. The water cages are described by the general notation X^n, where X = the number of sides of a cage face, n = the number of cage faces having these X sides. It is not necessary for all cages in these gas hydrate structures to be occupied, *e.g.* methane hydrate can be prepared with just 90% of the small cages occupied by methane.

The sI hydrate and sII hydrate structures are of particular importance in the gas industry because they encage small gas molecules that are found in natural gas. sI hydrate contains two different types of cavity: a pentagonal dodecahedral cavity (12-hedra, see Fig. 2a), denoted 5^{12} (comprising 12 pentagons), and a larger tetracaidecahedral cavity (14-hedra, see Fig. 2b), denoted $5^{12}6^2$ (comprising 12 pentagons and 2 hexagons). The packing in sI hydrate can be described as 5^{12} cavities sharing vertices, with no direct face sharing occurring between these 12-hedra. The vertices of the 14-hedra are arranged in columns in which 12-hedra occupy the space between each pair of 14-hedra. The unit cell of sII hydrate also contains two different types of cavity: a small 5^{12} cavity and a hexacaidecahedral cavity (16-hedra, see Fig. 2c), denoted $5^{12}6^4$ (comprising 12

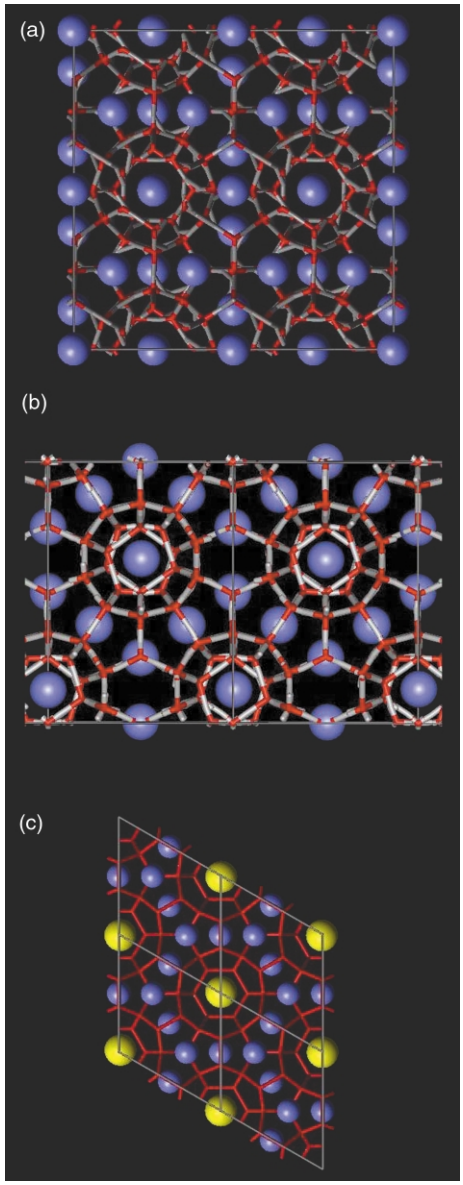

Fig. 1 Crystal structures of (a) sI hydrate; four unit cells viewed along a cubic crystallographic axis, (b) sII hydrate; two unit cells viewed along a face diagonal, and (c) sH hydrate; four unit cells viewed along the six-fold crystallographic axis (the positions of the hydrogen atoms have not been included; the large cavity, $5^{12}6^8$, has been highlighted by the yellow guest). All cavities are assumed to be filled in these figures.

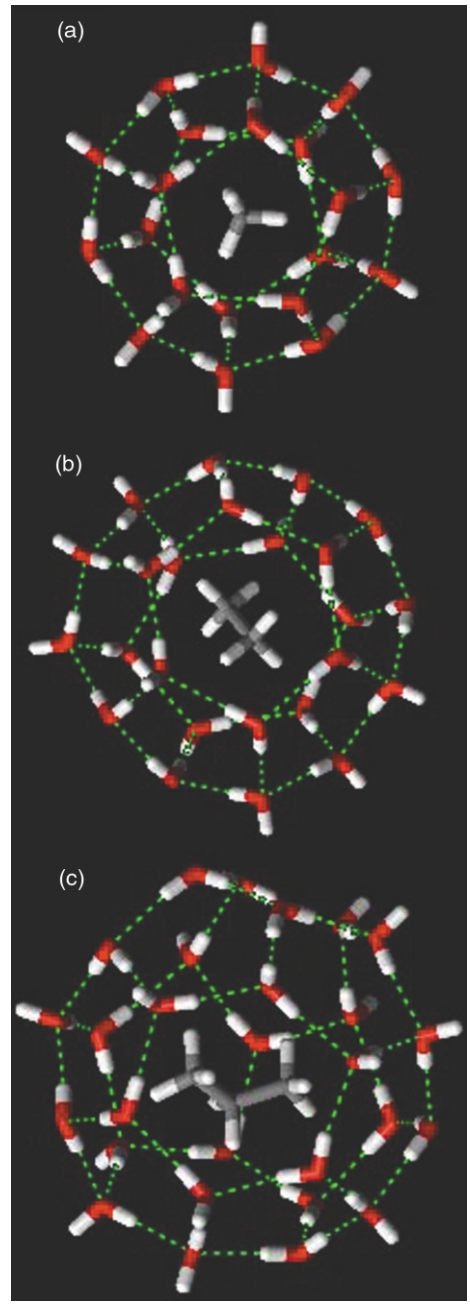

Fig. 2 Typical guest occupancies of the cavities of sI and sII hydrates: (a) a pentagonal dodecahedral cavity containing methane, (b) a tetracaidecahedral cavity containing ethane, and (c) a hexacaidecahedral cavity containing propane.

pentagons and 4 hexagons), which is slightly larger that the $5^{12}6^2$ cavity found in sI hydrate. The packing in sII hydrate can be described as 5^{12} cavities sharing faces in 3D, with the void spaces being occupied by the 16-hedra.

The crystal structures of sI hydrate and sII hydrate were first determined in the late 1940s and early 1950s by von Stackelberg

Table 1 Structural properties of clathrate hydrates

Property	sI	sII	sH	sT[a]
Lattice type	Primitive cubic	Face-centred cubic	Hexagonal	Trigonal
Space group	*Pm3n*	*Fd3m*	*P6/mmm*	*P*321
Unit cell parameters/nm	a = 1.20	a = 1.70	a = 1.21, c = 1.01	a = 3.50, c = 1.24
Average cavity radius/nm [number of cavities per unit cell (cavity type)]	0.395 [2 (5^{12})] (S) 0.433 [6 ($5^{12}6^2$)] (L)	0.391 [16 (5^{12})] (S) 0.473 [8 ($5^{12}6^4$)] (L)	0.391 [3 (5^{12})] (S) 0.406 [2 ($4^35^66^3$)] (S) 0.571 [1 ($5^{12}6^8$)] (L)	[12 ($4^25^86^1$)] (S) [12 ($5^{12}6^3$)] (L) [12 ($5^{12}6^2$)] (L) [24 ($4^15^{10}6^3$)] (L)
Ratio of numbers of small/large cavities	0.33	2	5	0.25
Number of water molecules per unit cell	46	136	34	348
Density/g cm^{-3}	0.91[b]	0.94[c]	1.952[d]	1.074[e]

[a] Full details of this structure have yet to be published. [b] Fractional occupancy of CH_4 (calculated from a theoretical model) in small (S) and large (L) cavities = 0.87 (S) and 0.973 (L).[3] [c] Fractional occupancy (calculated from a theoretical model) in small (S) and large (L) cages = CH_4: 0.672 (S), 0.057 (L); C_2H_6: 0.096 (L) only; C_3H_8: 0.84 (L) only.[3] [d] Calculated from single crystal X-ray diffraction data of 2,2-dimethylpentane 5(Xe,H_2S) 34H_2O. [e] Empty small cages and large cages filled with DME (calculated from single crystal X-ray diffraction data).[4]

and co-workers using X-ray diffraction.[3] This was followed by more extensive X-ray diffraction studies of these hydrate structures in 1965 by McMullan and Jeffrey,[5] and by Mak and McMullan.[6] These first clathrate hydrates are model gas hydrates [guest molecules: ethylene oxide (sI hydrate[5]) and tetrahydrofuran/hydrogen sulfide (THF/H_2S; sII hydrate[6]), respectively] which are stable at low temperature and atmospheric pressure. Therefore, unlike the situation with natural gas hydrates, aqueous solutions of ethylene oxide and tetrahydrofuran readily form hydrate single crystals at atmospheric pressure, whose structures can be readily determined using single crystal X-ray diffraction. THF hydrate is a particularly widely used model system in studies of gas hydrates since it readily forms, at atmospheric pressure, the same crystal structure (sII hydrate) as that formed (generally at elevated pressures) by several natural gas hydrates. Thus, a natural gas mixture consisting mainly of methane with about 3 vol% propane forms sII hydrate.

The sH hydrate structure (see Table 1 and Fig. 1c)[7] is important in the oil industry because the large cage (denoted $5^{12}6^8$, *i.e.* comprising 12 pentagons and 8 hexagons) in this structure can accommodate the larger molecules found in crude oils. Recently, a new hydrate structure, sT hydrate (Table 1), has been discovered[4] in which all the three types of large cages ($5^{12}6^3$, $5^{12}6^2$, and $4^15^{10}6^3$) in the structure are occupied by dimethyl ether guest molecules. In addition to the hydrate structures discussed in detail above, two new structures at higher pressures have been discovered, as discussed in the next section. It is in fact surprising that after over five decades since the first hydrate structures were characterised, so few different hydrate structures have been reported. Indeed, it is likely that more hydrate structure types will be discovered in the near future.

1.2 Occurrence of gas hydrates in space and comets

It has been suggested that natural gas hydrates also exist in space, in particular on Mars, Saturn, Uranus and Neptune. Far-infrared absorption measurements indicate that carbon dioxide hydrate is formed at 150 K, which has implications concerning the occurrence of this material at the Martian pole in the winter.[8]

Recently,[9] neutron and X-ray diffraction measurements were performed on methane hydrate up to 10 GPa. Samples were also compressed to 3 GPa at 130 K and warmed to room temperature with the pressure fixed at 3 GPa to simulate the conditions characteristic of the primordial core during the accretion of Titan (one of the moons of Saturn). The results indicate that Titan may contain stable phases of methane hydrate, with the suggestion that sI methane hydrate possibly contributes to atmospheric methane *via* convective processes such as cryo-vulcanism.[9] In particular, at 1.1 GPa the neutron diffraction pattern indicates the presence of ice VI and a new methane hydrate phase, MH-II, which has a different crystal structure to sI hydrate. Methane hydrate under 'normal' pressure and temperature conditions forms sI hydrate. Between 2.0 and 10 GPa, another new methane hydrate phase was identified, MH-III, which was shown to be richer in methane than MH-II. The crystal structures of MH-II and MH-III were determined from synchrotron X-ray powder diffraction data. MH-II was indexed with a hexagonal crystallographic unit cell (with an estimated water : methane composition of 3.5 : 1), a = 1.179 and c = 0.992 nm at 1.7 GPa. MH-III was indexed with a body-centred orthorhombic crystallographic unit cell (containing eight water molecules and four methane molecules) of dimensions: a = 0.475, b = 0.806, and c = 0.785 nm at 3.0 GPa.

These recent results[9] indicate that a mixture of ice and MH-III may have been present in the primordial core at similar pressure and temperature conditions to those which existed at the end of accretion. In addition, because of the readily reversible nature of the transitions from sI methane hydrate to MH-II and MH-II to MH-III, the authors propose that all core methane was transformed to sI methane hydrate after core overturn, resulting in an approximately 100 km thick layer of sI methane hydrate within the ice mantle of Titan.

Conversely, using X-ray microprobe and Raman spectroscopy to study the transformations in methane hydrate at high pressure, Chou *et al.*[10] have shown that sI methane hydrate transforms to an sII hydrate phase at 100 MPa and an sH hydrate phase (*cf.* the hexagonal phase of MH-II in ref. 9) at 600 MPa. Chou *et al.* suggest that these new phases of methane hydrate may be also present in the outer planets and their satellites. It should be noted that these two studies[9,10] followed very different temperature and pressure profiles.

1.3 Industrial significance of gas hydrates

Natural gas hydrates (sI, sII and sH) are important industrially because the formation of these solids in gas and oil production and transmission pipelines (*e.g.* subsea pipelines) can lead to blockage, which can stop production and compromise the structural integrity of both the pipelines and surface facilities.[11] This can lead to catastrophic economic loss and ecological risks, as well as potential safety hazards to exploration and transmission personnel.

To prevent the formation of hydrates in pipelines, the conventional control strategy is to use 'thermodynamic' inhibitors, such as methanol, generally at high concentrations (*e.g.* 40 vol%). This type of inhibitor operates by shifting the hydrate formation phase boundary away from the temperature and pressure conditions of the process in question, increasing the driving force required for hydrate formation (see Fig. 3). However, the use of thermodynamic inhibitors is both uneconomical and ecologically unsound. With current industry trends moving oil and gas production to deeper waters (which represent more favourable hydrate forming conditions), up to 60 vol% methanol could be required for effective hydrate control.

The costs associated with methanol addition alone are not trivial, as illustrated in the following example:[12] for a relatively small two-well satellite field, the water solubility at reservoir conditions of 379 K and 33 MPa is 5.57 kg/1000 m^3. For a gas flow rate of 5.66×10^6 m^3 per day, the mass of water associated with this gas is 3.155×10^4 kg per day. For these reservoir conditions, 0.65 kg of methanol is required for each kg of water in order to prevent hydrate formation. Therefore, the amount of methanol required for this small field is 2.051×10^4 kg per day, which equates to methanol costs of around $5 million per year. Clearly the economic implications of this method of preventing hydrate formation are considerable.

An alternative technology to control hydrate formation within pipelines is to use low-dosage 'kinetic' inhibitors which are effective at concentrations of about 0.5 vol%. These new inhibitors are designed either to delay hydrate formation (such that the time required for the hydrate to form is longer than the residence time of the gas in the pipeline) or to modify the hydrate crystal morphology (such that only very small hydrate particles are formed which can be easily pumped through the pipeline). Clearly, major improvements in controlling hydrate formation, both economic and ecological, can be made if a suitable cost-effective low-dosage inhibitor can be found (further details on hydrate inhibition studies are given in Section 3).

1.4 Technological importance of gas hydrates

In addition to the problems incurred by the presence of gas hydrates in pipelines, there are a number of technologically

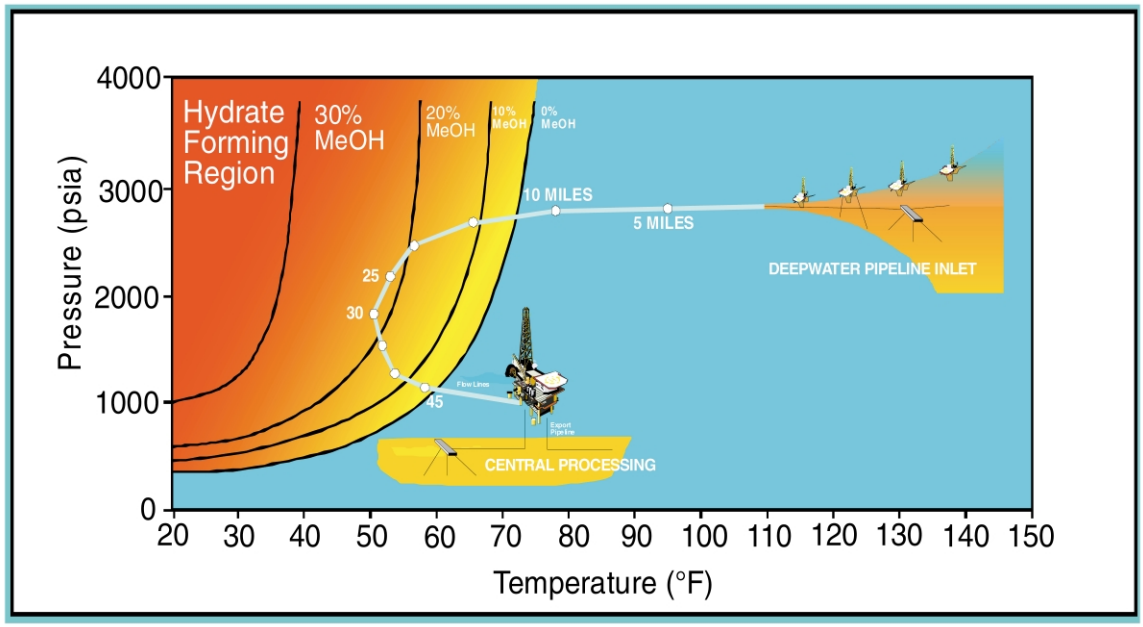

Fig. 3 A composite diagram showing, on the left: the phase boundary of methane hydrate formation as a function of temperature and pressure. The black lines show the phase boundary line shifting to the left on the addition of increasing methanol concentration. On the right: the blue region is that where hydrate crystals are not formed and superimposed over this is a pipeline of about 45 miles in length containing natural gas.

important applications of gas hydrates, such as in separation processes, fuel transportation and storage, and as a potential fuel resource. In particular, natural deposits of predominantly methane hydrate in permafrost, ocean trenches and continental margins provide a possible future fuel resource.[13] From acoustic methods, such as bottom-simulating reflector (BSR) profiles and drilling programmes conducted by the US Geological Survey, as well as regional geological information, the amount of gas in the form of gas hydrate in off-shore and on-shore sediments has been estimated to be much larger than global combined fossil fuel reserves [one cubic metre of methane hydrate in which 90% of the cages are occupied contains the equivalent of 156 m^3 of methane under standard conditions (STP)]. The mean estimate of the amount of gas in the form of gas hydrates for the entire US has been calculated to be around 9×10^{21} m^3.[14] These methane hydrate deposits originate from the microbial breakdown of organic matter which has occurred over millions of years. A fascinating recent finding by oceanographers[15] is the identification of a new iceworm species (*Hesiocaeca methanicola*, from the polychaete family *Hesionidae*), which is able to burrow into gas hydrate deposits buried by up to 0.1 m of sediment. An important issue is whether these iceworms exist symbiotically with bacteria which use hydrocarbon molecules such as methane in their chemosynthetic processes.

Understandably, the estimated scale of these deposits to date has generated much interest amongst energy suppliers, the US Department of Energy, and the Japanese New Energy and Industrial Technology Development Organisation (NEDO) as the sheer volume of methane hydrate may provide a long-term solution to depleting natural resources available at present. However, exploitation of these submarine gas hydrates requires extensive research and caution in developing the technology to extract methane from these deposits. In addition, stringent considerations need to be made to the economics, safety, and the possible environmental and ecological impacts. The natural release of methane into the atmosphere from such methane deposits is not significant at present, but the effects may be large in the future, particularly during exploration, and may contribute to a positive feedback mechanism for global warming. This mechanism is also believed to have been a major contributor to the warming that occurred at the end of the last major glacial period.[16]

Turning to consider other technological aspects, gas hydrate formation has been applied to separation processes, in particular the treatment of aqueous and gaseous pollutant streams. Kang and Lee[17] demonstrated the use of gas hydrates for recovering more than 99 mol% CO_2 from a power plant flue gas (typically consisting of a ternary mixture of CO_2, O_2, and N_2 after pre-treatment). These studies showed that a gas mixture containing 17 mol% CO_2 and 83 mol% N_2 could form gas hydrates with water at 275 K and around 0.5 MPa when 1 mol% THF was added to the aqueous solution as a gas hydrate promoter. This represents a dramatic decrease in driving force in comparison with the case in which THF is absent, for which the equilibrium dissociation pressure is around 8.4 MPa at 275 K. The recovery of CO_2 gas was increased by dissociating the gas hydrates (containing THF, which gives a relatively small composition difference of CO_2 between vapour and hydrate phases compared to a THF-free aqueous system) formed in the first reaction vessel into a second reaction vessel in which gas hydrates were re-formed, this time in the absence of THF.

To progress with understanding and tackling some of the technological challenges relating to controlling the crystal growth, inhibition and decomposition of natural gas hydrates, it is essential to develop a fundamental understanding of the molecular mechanisms involved. Understanding these issues is also important within the broader field of inclusion chemistry. The remainder of this article is focused on the application of a range of physico-chemical techniques and approaches for studying natural gas hydrate crystal growth, inhibition, and decomposition. As such, this article is complementary to other reviews in this field, which have focused more on the applied, engineering and technological aspects of clathrate hydrates.[11,18]

2 Gas hydrate formation

2.1 Phase equilibria studies of gas hydrates

Most of the previous work on natural gas hydrate formation has concentrated on making macroscopic time-independent measurements to determine the equilibrium properties of gas hydrates (including that from the laboratories of Kobayashi;

Holder; Ng and Robinson; Sloan), or performing model calculations. These phase equilibria studies have been previously reviewed by Sloan.[3] Macroscopic measurements of gas hydrate phase equilibria have mainly focused on gas consumption or pressure drop measurements as a function of temperature. Gas consumption *versus* temperature plots obtained during gas hydrate formation and decomposition are found to exhibit a characteristic hysteresis, as illustrated in Fig. 4 for methane hydrate. It has been suggested that this hysteresis may be attributed to 'residual' hydrate structures.[19]

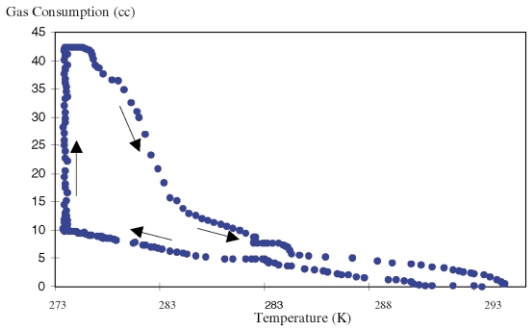

Fig. 4 Gas consumption *versus* temperature for methane hydrate formation (indicated by up-arrows) and decomposition (indicated by down-arrows) at 3.01 MPa, T = 293.1 to 273.7 K.

The first thermodynamic model to predict gas hydrate phase equilibria was developed using statistical mechanics by van der Waals and Platteeuw in 1958,[20] and is analogous to the commonly used model for describing ideal localized adsorption. The main assumptions included in this model are: (i) a cavity can only hold one guest molecule; (ii) the motion of a guest molecule in its cage is independent of the number and types of guest molecules present; (iii) interactions between host and guest molecules are weak van der Waals forces and extend only to the first shell of water molecules around each guest molecule (with the neglect also of guest–guest interactions between different cages); (iv) the hydrate lattice is not distorted by the guest molecule.

The relationship between equilibrium vapour pressure (or fugacity, f_K) of solute K, composition (y_{K_i}, guest occupancy or the probability of finding a solute molecule K in a host cavity of type i), and chemical potential of the solvent (water molecules) in a clathrate (μ_Q) is given, according to the van der Waals and Platteeuw model, by eqns. (1) and (2):

$$y_{K_i} = \frac{C_{K_i} f_K}{1 + \sum_J C_{J_i} f_J} \quad (1)$$

$$\mu_Q = \mu_Q^\beta + kT \sum_i \nu_i \ln\left(1 - \sum_K y_{K_i}\right) \quad (2)$$

where C_{K_i} is an equilibrium constant (or Langmuir constant) for the Kth type of guest (or Jth type of guest for C_{J_i}) in the i^{th} type of cavity, μ_Q^β is the chemical potential of the metastable empty hydrate lattice, and ν_i is the number of cavities of type i per water molecule in the hydrate lattice.

The van der Waals and Platteeuw model performs well near the ice point of water, but deviations are significant far from the normal ice point. Despite its limitations and simple assumptions, this first model has provided the basis of all subsequent models developed to predict the phase equilibrium properties of gas hydrates.[11] In particular, the van der Waals and Platteeuw model was extended by Parrish and Prausnitz in 1972[21] for multi-component mixtures. This extension was later simplified by Holder and Grigoriou.[22] Recently, Klauda and Sandler[23] in 2000 developed a classical thermodynamic approach to predict hydrate phase behaviour which removes the need for reference energy parameters, as used in the van der Waals and Platteeuw type models, and thereby increases the accuracy of the predictions of equilibrium pressures for gas hydrate formation.

Westacott and Rodger[24] have developed a method based on the phonon properties of crystals that can be used to directly calculate the free energy of the water lattice, removing the assumption that there is no lattice relaxation in the van der Waals and Platteeuw theory. Also, coupled with an equation of state, this method can be used to calculate hydrate phase diagrams. Zele *et al.*[25] have also developed a thermodynamic model which takes into account the effect of lattice stretching due to guest size on the reference chemical potential difference between the empty hydrate lattice and water (liquid water or ice). This new reference chemical potential difference was calculated using constant pressure molecular dynamics simulations and has been used to predict the equilibrium conditions for single component and multi-component gas hydrates. The molecular simulations showed that the hydrate lattice expands slightly in the presence of larger guest molecules, which is in agreement with the findings obtained from other experimental studies, *e.g.* the calculations show that the lattice constant for krypton hydrate (sII hydrate) is 1.69 nm and increases to 1.76 nm for isobutane hydrate (sII hydrate).

Structural phase equilibria data for sI and sII hydrates have been obtained using Raman spectroscopy[26] and ^{13}C and ^{129}Xe NMR spectroscopy.[27] In particular, the phase transition from sI to sII hydrate has been identified for a binary ethane–methane gas mixture. It was found that although methane and ethane each form sI hydrate, sII hydrate is formed when the proportion of methane in a mixture with ethane is 75 mol% or higher at 274.2 K and around 1 MPa.[26] The transition from sI to sII hydrate was identified from the Raman C–H resonance doublet of ethane which occurs at 2891.2 and 2946.2 cm^{-1} for ethane in the large cavity of sI hydrate and at 2887.3 and 2942.3 cm^{-1} for ethane in the large cavity of sII hydrate. The ν_1 symmetric C–H stretch of methane is also indicative of the type of hydrate structure formed since its frequency depends on the type of cavity it occupies and the relative intensities of the ν_1(C–H) peaks due to methane occupying the large and small cavities depends directly on the relative occupancies of these cavities (the ratio of large : small cavities occupied by methane is 3 : 1 in sI hydrate and 1 : 2 in sII hydrate). The hydrate structure type can be also confirmed using ^{13}C CP MAS NMR: for example, ethane occupying the large cage of sI has a chemical shift of 7.7 ppm, and ethane in the large cage of sII has a chemical shift of 6.4 ppm.

Sum *et al.*[28] have also used Raman spectroscopy to determine the relative occupancies of the large and small cavities and the hydration number (n) for single and double hydrates (containing one and two types of guest molecules, respectively), including: CH_4 (sI hydrate), CH_4 and TDF (THF-d_8; sII hydrate), CH_4 and CO_2 (sI hydrate), CD_4 and C_3H_8 (sII hydrate). An important assumption of Raman measurements of the cage occupancy and hydration number is that the Raman scattering cross section of the guest species does not change when it is incorporated into the hydrate host structure. For CH_4 hydrate, it was found that the large cages are almost fully occupied and the small cages are 90% occupied, whereas for CO_2 hydrate, only the large cages were found to be occupied. For the double hydrate of CH_4–CO_2, most of the large cages accommodate both types of guest molecule, although less CH_4 is present in the large cages since CO_2 only occupies the large cage, while CH_4 can occupy both the large and small cages. Good agreement was obtained between these measured hydrate compositions and those predicted using the van der Waals and Platteeuw model. Guest occupancies for single and double hydrates have also been studied by Ripmeester *et al.* using ^{129}Xe NMR spectroscopy.[27]

Morita *et al.*[29] also used Raman spectroscopy to study the structure and stability of ethane hydrate from 290 to 324 K and 20 to 479 MPa. The authors reported that ethane molecules can

occupy both the small and large cavities of sI hydrate at 300 MPa, although the occupancy of the small cavity is very low at pressures lower than 100 MPa. The intermolecular (O–O) vibrational mode of hydrogen-bonded water in the ethane hydrate crystal was found to have a half-width of around 40 cm^{-1} and is independent of pressure, whereas for carbon dioxide hydrate and methane hydrate the corresponding mode is strongly dependent on pressure and has a half-width of around 30 cm^{-1}.

The dynamic properties of the guest molecules and the water molecules in gas hydrates have been extensively studied using solid state NMR spectroscopy.[27] The water molecule reorientation process was found to be dependent on the nature of the guest molecule, *e.g.* the activation energies and reorientational times for the water dynamics have been found to be much lower for guest molecules that contain oxygen atoms than those that do not.[27] This observation suggests that the guest molecules may be involved in establishing a transient hydrogen bond with the water molecules. A recent solid state ^2H NMR spectroscopic study on a model sII gas hydrate, THF hydrate, over the temperature range 125 to 243 K,[30] has shown that the THF molecules reorient rapidly in comparison to the dynamics of the water molecules. At least two dynamically distinguishable types of water molecule have been identified,[30] both undergoing a four-site tetrahedral jump motion, but with different jump rates (jumps involve the movement of the deuterons of a D_2O molecule between sites that represent hydrogen bonding to a tetrahedral arrangement of neighbouring D_2O molecules). It was also proposed that there is a distribution in terms of anisotropic characteristics associated with the reorientational motions of different guest molecules, reflecting the fact that the dynamics of the water molecules is substantially slower than the guest dynamics, such that different guest molecules experience a distribution of local water cage structures.

2.2 Macroscopic time-resolved measurements

Significant and high quality kinetic data during gas hydrate formation have been obtained in a number of laboratories including those of Bishnoi, Englezos, Sloan, and Skovborg.[3] Recently, Servio *et al.*[31] used light scattering to measure the nucleation and crystal growth of ethane hydrate in a stirred sapphire reactor cell. In some of their measurements they were able to overcome the inherent experimental difficulties of using light scattering to measure hydrate nuclei which are very small by growing the hydrate nuclei on positively and negatively charged latex spheres (600 and 692 nm diameter, respectively) suspended in water. It was expected that hydrate nucleation would preferentially occur on the latex spheres rather than in bulk water due to the lower energy barrier for nucleation. The nucleation induction times for a water–ethane mixture at 278.3 K and 1300 kPa were approximately 130 minutes in the absence of latex particles, 163 minutes in the presence of positively charged latex spheres, and 93 minutes in the presence of negatively charged latex particles. It therefore seems that the negatively charged latex particles promote the formation of ethane hydrate, whereas the positively charged latex particles delay the formation of ethane hydrate.

Despite the progress made so far in kinetic studies of gas hydrate formation, it is clear that there still remains a need for extensive kinetic studies to be performed, using both macroscopic and microscopic techniques, in order that improved and more accurate kinetic models can be developed for hydrate formation and decomposition.

2.3 Mechanistic models

Only a few groups have developed mechanistic models for gas hydrate nucleation and crystal growth, and these models have been proposed using macroscopic experimental kinetic data obtained during gas hydrate formation.[19,32] The main reasons for the limited kinetic data and hence inaccurate kinetic models are the stochastic nature and apparatus dependence of hydrate formation. The stochastic nature of crystallisation processes at low driving force conditions is a well-known phenomenon of heterogeneous nucleation, where induction times generally have large variations, and can range from a few seconds to 167 minutes or greater.

The nucleation process is the first step in gas hydrate formation in which water and gas molecules in a supersaturated solution (generally at the gas–water interface) re-organize to form a hydrate nucleus of a critical cluster size, which is stable and from which the growth of hydrate crystals can proceed. The critical cluster of a hydrate particle is formed within the nucleation induction time.

Sloan *et al.* proposed a mechanistic model for gas hydrate nucleation from liquid water which could be related to a pressure–temperature phase diagram.[19] The evolution of gas hydrate crystals is proposed to start with the interaction of liquid water with gas molecules to form small and large labile clusters which resemble the hydrate cages. Either these clusters may grow to hydrate unit cells or agglomerations of hydrate unit cells, or the clusters can shrink and dissipate. These species are termed metastable since they are below the critical cluster size for hydrate growth. When the nuclei reach a critical radius, the hydrate crystals are stable and secondary nucleation can occur, followed by rapid hydrate crystal growth.

An intrinsic kinetic model (with just one adjustable parameter) was proposed by Englezos *et al.* for methane hydrate and ethane hydrate crystal growth. This model was based on macroscopic kinetic measurements performed from 274 to 282 K and from 0.636 to 8.903 MPa.[32] Constant pressure gas consumption and solubility measurements were performed in a stirred reactor during hydrate formation. The rate of gas dissolution in the water phase was used to estimate the liquid mass transfer coefficient and the concentration of dissolved gas in equilibrium with the partial pressure of gas at the liquid–gas interface. Primary or spontaneous homogeneous nucleation (in the absence of foreign particulates) was assumed to proceed with the initiation of a 'clustering process' during which gas molecules are incorporated into water cavities. The formation of primary nuclei was identified by the appearance of turbidity in the water–gas solution. In this model[32] it is assumed that the nuclei form instantaneously and that primary nucleation ceases after the appearance of turbidity. This is because the energy barrier to form a new nucleus is higher than that to incorporate gas molecules into existing nucleation centres. The model allows for the generation of new hydrate particles during the growth period by secondary nucleation which arises from hydrate particle–particle interactions, hydrate particle–reactor wall interactions and hydrate particle–stirrer interactions. The overall driving force for the crystallisation process is given by the difference in fugacity of the dissolved gas and the three-phase equilibrium fugacity at a specific temperature.

Crystal growth was proposed to proceed *via* two main steps. The first step involves diffusion of dissolved gas molecules to the crystal–liquid interface *via* the 'laminar diffusion layer' around the hydrate crystal. The second step involves adsorption of gas molecules into the water network at the interface and stabilization of the water lattice. Gas hydrate crystal growth occurring in the liquid phase is a first-order irreversible (pathway) homogeneous reaction. In this model, the hydrate particles are assumed to be spherical. Although the conditions within the experimental reactor are clearly not homogeneous, the assumption of homogeneous nucleation can be justified since the hydrate particle is generally three orders of magnitude smaller than the diffusion film for gas adsorption. There was generally good agreement between the experimental gas consumption data and the calculated data, except where the

homogeneous nucleation rate constant exceeded 10^{12} nuclei m^{-2} s^{-1}.

Despite the progress made so far on the development of mechanistic models for hydrate nucleation[19] and hydrate growth,[32] there remains a need for these mechanistic models to be verified with molecular-level experimental data. Important experimental studies that are starting to tackle this challenging task are discussed in the next section.

2.4 *in situ* Spectroscopic and diffraction studies

in situ Raman spectra have been recorded by Sloan *et al.*[33] during methane hydrate formation from a methane–water mixture at a constant pressure of 31.7 MPa and cooling at a rate of 0.1 K min^{-1} from 297 to 275.5 K. At the start of the hydrate formation process, only one Raman peak at 2911.3 cm^{-1} is present, and is attributed to methane dissolved in water. After around 83 minutes, there is a smooth transition to two peaks at 2905 and 2915 cm^{-1} attributed to methane molecules in the large and small cavities of sI hydrate, respectively. The ratio of large : small cavities occupied by methane was determined from the ratios of the integrated intensities of the two peaks at 2905 and 2915 cm^{-1} (*cf.* ref. 26). The final ratios of large : small cavities occupied for the uninhibited methane hydrate and methane hydrate inhibited with a kinetic inhibitor, poly(*N*-vinylcaprolactam) (PVCap; 0.02 vol%), were about 3.2 (close to the totally occupied equilibrium value of 3.0) and about 2.4, respectively. The results suggest that PVCap affects the rate of formation of hydrate cavities. We have observed a similar effect for methane hydrate grown in the presence of a model kinetic inhibitor, poly(*N*-vinylpyrrolidone) (PVP) using Raman spectroscopy.

The first time-resolved energy dispersive synchrotron X-ray diffraction studies of gas hydrate formation, decomposition and inhibition[34] were performed for propane hydrate and carbon dioxide hydrate in a stainless steel high pressure, low temperature stirred reactor (see Fig. 5). Fig. 6 shows the gradual evolution of propane hydrate from a liquid water–propane gas mixture. These studies showed that the lattice parameters at around 273 K and 0.43 MPa (for propane (sII) hydrate) and 3.29 MPa (for carbon dioxide (sI) hydrate) are slightly different to those obtained from previous low temperature, atmospheric pressure X-ray diffraction measurements on single crystals of clathrate hydrates, although the crystal structures are the same for both sets of conditions. The lattice constants for carbon dioxide hydrate and propane hydrate determined *in situ* were 1.193 and 1.720 nm compared to 1.207 and 1.740 nm (measured by von Stackelberg *et al.* at 77 K and atmospheric pressure[3]), respectively. The slightly lower values observed in the *in situ* measurements could be attributed mainly to the effect of the type of guest molecule present. Recent single crystal X-ray diffraction measurements on carbon dioxide hydrate at 173 K gave a lattice constant of 1.189 nm,[35] which is in good agreement with the *in situ* lattice constant of 1.193 nm.[34]

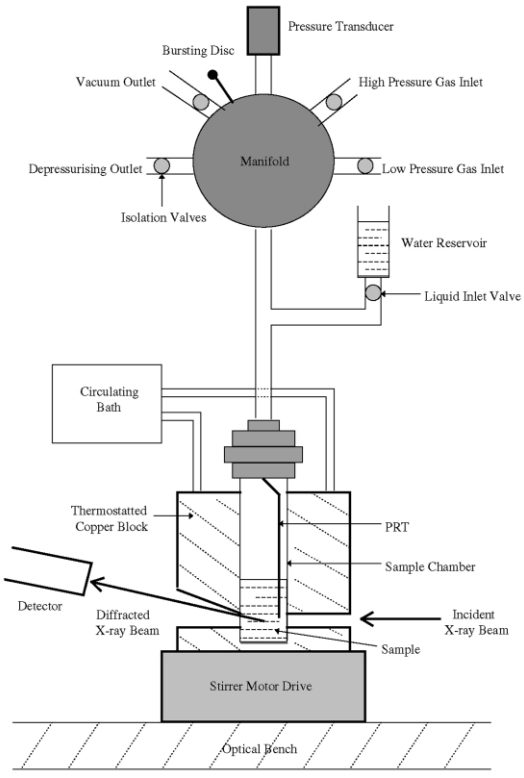

Fig. 5 Schematic of an *in situ* synchrotron X-ray cell for studying gas hydrate formation.[34]

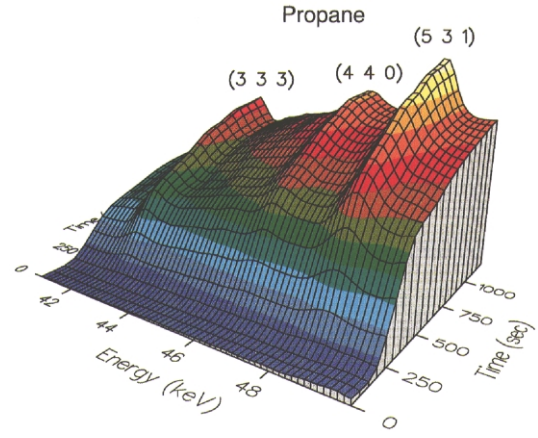

Fig. 6 X-Ray diffractograms collected at $2\theta = 5.04°$ as a function of time during propane hydrate formation. The vertical axis is diffraction intensity in arbitrary units.

Henning *et al.* have performed *in situ* neutron diffraction studies of carbon dioxide hydrate formation from ice[36] at 230 to 276 K and around 6.2 MPa. Only around 50–70% conversion of ice to hydrate was generally observed, although around 98% conversion could be achieved when the temperature was slowly increased above the melting point of ice and then maintained under pressure at 276.8 K. It was proposed from these measurements that after the initial period of fast conversion to hydrate on the surface of the ice particles, the process is controlled by diffusion of carbon dioxide molecules through the hydrate layer. After diffusion through the hydrate layer, hydrate formation proceeds from carbon dioxide and water molecules in a quasi-liquid layer (or pre-melting layer). This is in agreement with the findings of Stern *et al.* who reported enhanced methane hydrate formation at a liquid-like surface film on fine ice grains (about 200 μm) from optical cell experiments.[37] Stern *et al.* suggest that significant hydrate nucleation requires surface melting, while growth (which is limited under ice subsolidus conditions) requires continued nucleation of the melt at the hydrate–mantle/ice-core interface. Henning *et al.*[36] also found that carbon dioxide occupies both the small and large cavities of sI hydrate, with the large cavity having a higher occupancy than the smaller cavity, although occupancy of the small cavity was found to depend on the thermal conditions. Variations in the cage occupancies in carbon dioxide hydrate determined by different groups have been attributed to the different methods of sample preparation.[36]

Neutron diffraction with H/D isotopic substitution, using the small angle neutron diffractometer for amorphous and liquid samples (SANDALS) at ISIS (Rutherford Appleton Laboratory), has been used to investigate the structure of water molecules around dissolved methane molecules during methane hydrate formation.[38] The derived carbon–oxygen pair correlation functions for five cases before, during and after hydrate formation under different conditions of temperature and

pressure are given in Fig. 7. The typical carbon–oxygen distance in the liquid is about 3.5 Å and does not change significantly until methane hydrate has formed. The hydration

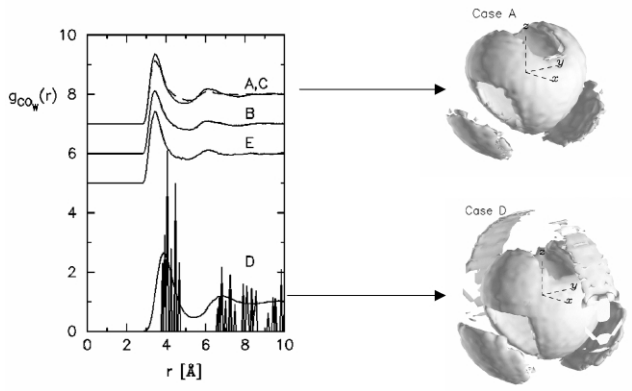

Fig. 7 Left side: pair correlation functions during methane hydrate formation. A–D are at 14.5 MPa, A at 291 K (before hydrate formation), B at 283 K, C at 277 K, D at 277 K (further into the hydrate formation process); E is at 3.4 MPa and 277 K (during methane hydrate formation). Right side: density of orientation of water molecules before and after hydrate formation.[38]

sphere around methane in the crystalline hydrate was confirmed to be significantly larger (by about 1 Å in diameter) than the hydration sphere around methane in the liquid. The coordination number of water molecules around methane is about 16 ± 1 water molecules in the liquid, which is significantly smaller than the value of 21 ± 1 water molecules after hydrate has formed (the expected value is 23 for sI hydrate). The subtle differences in the methane–water correlations at the onset of hydrate formation (B, C and E; Fig. 7) indicate that once hydrate starts to form, the hydration shell becomes slightly less ordered on average, compared to the methane–water system above the hydrate formation temperature. In addition, the methane–methane correlations show that methane molecules can adopt a range of separations, corresponding to the more disordered nature of the methane–water correlations.

Bowron *et al*. also examined the structure of the hydration sphere around krypton atoms in liquid water and solid krypton hydrate using extended X-ray absorption fine structure (EXAFS) spectroscopy.[39] The liquid-to-solid phase transition was indicated by an increase in amplitude and long-range order of the refined Kr–O partial pair correlation function, $g(r)$, derived from the solid-state EXAFS spectrum. By constraining the radius of the small cage to 3.902 Å (consistent with either sI or sII hydrate) in the crystalline hydrate, the radius of the large cage was refined to 4.9 Å, which corresponds to sII hydrate. The coordination number of water molecules around Kr was around 13 in the liquid and around 12.5 in the solid. The full width at half maximum of the first peak in the $g(r)$ plot was found to be 0.9 and around 1.1 Å in the crystalline and liquid states, respectively. This was interpreted as the hydration cage in the liquid being more loosely defined and disordered compared to the hydration cage of the crystalline hydrate, in agreement with the studies reported by Koh *et al*.[38] on the liquid state structure of methane hydrate.

2.5 Molecular simulation studies

The structural evolution of methane hydrate has been also studied using molecular dynamics (MD) simulations by Baez and Clancy.[40] In these simulations, the three-site rigid simple point charge (SPC/E) and Lennard–Jones (L–J) potential models were used to describe the water and gas (methane) molecules, respectively.[40] A sI hydrate crystal was implanted into an sI hydrate melt. Crystal growth was allowed to proceed at 220 K and 60 MPa. From video animation, it was shown that partial cavities form on the template of the fixed crystal seed during the simulation. The MD simulations were also performed during sI hydrate dissociation at 270 K and 4 MPa and showed that partial cavities exist for up to around 140 ps during the simulation, with a pentagonal dodecahedral cavity being the last structure left before melting is completed.[40]

Methane hydrate nucleation was also studied by Westacott and Rodger using hydrate clusters containing up to 184 molecules at 270 K and 500 MPa.[41] In this study, free energy minimisation was performed using the local molecular harmonic model (LMHM), with SPC and L–J potentials to describe water and methane, respectively. Significant distortion of the clusters was observed, similar to that found by Baez and Clancy. These LMHM calculations showed that clusters based on hexacaidecahedral cavities have the lowest free energy and hence are the most stable clusters. A critical cluster size of around 550–600 water molecules was found under these conditions (at the liquid side of the water–gas interface), compared to a critical cluster size of approximately 10^4 water molecules for methane hydrate formation from the gas phase.[41]

Evidence of relatively strong guest–host vibrational interactions for methane hydrate has been obtained from molecular dynamics and lattice dynamics calculations.[42] It was proposed that the localised rattling vibrations of the guest molecule are modulated by the host lattice vibrations and the avoided crossing between the crystal acoustic and guest vibrations may be the mechanism for transfer of energy between host and guest species. Tanaka *et al*.[43] however, found from free energy calculations that the anharmonic vibrations due to guest molecule rotations are the major contributor to the large thermal expansivity of gas hydrates (calculated thermal expansivities for ice Ih and the empty hydrate are lower than that of the occupied hydrate), while the contribution of the guest interaction energy (including host–guest interactions and guest–guest interactions) is much smaller and in fact reduces the thermal expansion of gas hydrates.[43]

3 Hydrate inhibition

Alternative technologies that can be used to control gas hydrate formation in gas and oil transportation and production pipelines include pipeline heating, pipeline coatings, or the addition of low-dosage chemical inhibitors. Low-dosage chemical inhibitors are a particularly attractive alternative technology to the industry, both economically and environmentally (as mentioned in Section 1), and include (see Fig. 8) polymer molecules, such as PVP, poly(*N*-vinylpyrrolidone), VC-713, the terpolymer of *N*-vinylpyrrolidone, *N*-vinylcaprolactam and dimethylaminoethyl methacrylate, and anti-agglomerants (quaternary ammonium salts).

3.1 Macroscopic inhibition studies

A few studies have been performed to examine the effect of polymer inhibitors on gas hydrate formation using macroscopic measurements, such as gas consumption (or pressure drop) measurements as a function of time[33] and dynamic light scattering. It was found that the polymer inhibitors are able to inhibit gas hydrate formation by several degrees of sub-cooling and suppress crystallisation for long periods of time at intermediate levels of sub-cooling. The effectiveness of polymer inhibitors has been also shown, by gas consumption measurements, to be enhanced through the addition of glycol ethers (*e.g.* 2-butoxyethanol, 0.75 vol%) with induction times for hydrate growth being increased by over 1100 min in some cases.[44] Nevertheless, the mechanism of hydrate inhibition still

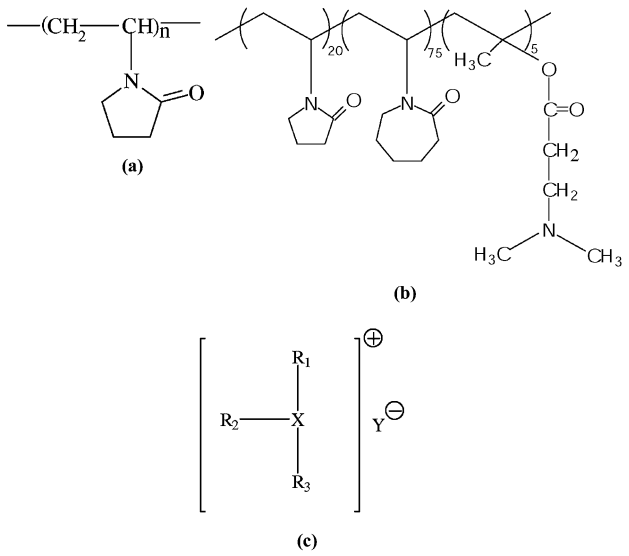

Fig. 8 Molecular structures of (a) PVP, (b) VC-713, and (c) an ammonium salt, where X is N–R_4 (R_4 can be hydrogen or an organic substituent), R_1, R_2 and R_3 are independently chosen from the group consisting of *n*-butyl, isopentyl or *n*-pentyl, and Y^- is an anion (counter-ion), such as a halide, sulfate or carboxylate.

remains unclear from these macroscopic measurements. To obtain a fundamental understanding of the mechanisms of hydrate inhibition will rely upon the future application of a complementary range of microscopic techniques, including ^{2}H NMR spectroscopy, Raman spectroscopy, X-ray and neutron diffraction and molecular simulation.

3.2 Structural inhibition studies

The kinetics of gas hydrate formation in the presence of polymer inhibitors has been also studied using Raman spectroscopy[33] and energy dispersive X-ray diffraction.[34] The Raman studies revealed that the ratio of occupation of the large : small cavities of methane hydrate was reduced from 3.0 to under 2.5 on addition of a polymer inhibitor, while both studies indicated that the hydrate host crystal structure is not changed in the presence of the inhibitor.

A number of studies have suggested that the mode of hydrate inhibition by polymer inhibitors is *via* adsorption of the polymer molecules onto the gas hydrate crystal surfaces[34,45–47] (see Fig. 9). Carver *et al.*[45] showed from Monte Carlo computer

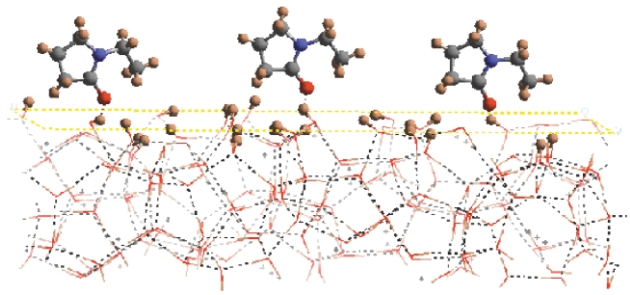

Fig. 9 Adsorption of the monomer unit of PVP on the {111} crystal surface of sI hydrate obtained from Monte Carlo simulation using the sorption module of Cerius^2 (MSI). Hydrogen atoms on the crystal surface are emphasized.

simulations that monomer and dimer units of PVP are strongly adsorbed on the {001} faces of methane hydrate, *via* hydrogen-bond formation at hydrate growth sites, depending on the availability of pendant hydrogens on the crystal surface, and also van der Waals interactions (although these interactions generally had a secondary effect on the adsorption geometry). Further confirmation of the adsorption mechanism of polymer inhibitors was provided by single crystal studies of a model sII hydrate (THF hydrate). These studies showed that polymer inhibitors, such as PVP, PVCap, or VC-713 change the hydrate crystal growth habit from octahedral crystals to two-dimensional hexagonal plates. The latter were thought to be the result of polymer adsorption onto the crystal surface.[46] The adsorption of polymer inhibitors on an sI hydrate surface was also inferred from single crystal experiments of a model sI hydrate (ethylene oxide hydrate). These studies showed that the crystal growth habit for sI hydrate changes from rhombic dodecahedral crystals (in the absence of an inhibitor) to highly-branched crystals (in the presence of a polymer inhibitor).[46]

Evidence of polymer adsorption on a model sII hydrate surface (THF hydrate) was also obtained by King *et al.*[47] from small-angle neutron scattering for four polymer inhibitors PEO [poly(ethylene oxide)]; PVP; PVCap; VIMA/VCap, *N*-methyl-*N*-vinylacetamide/*N*-vinyl-2-caprolactam copolymer.[47] Examining the polymer solutions (about 0.5 vol% of polymer in a TDF–D_2O solution) at 280 K (which is above the THF hydrate formation temperature), they found that all four polymers exhibit conformations typical of a polymer in a good solvent. However, each of the polymer solutions exhibits a rise in low-q scattering (where $q = 4\pi\sin(\theta/\lambda)$; 2θ = scattering angle, λ = neutron wavelength; the data were averaged radially to obtain the differential scattering cross-section as a function of q). This was attributed to the presence of aggregates of the polymer. On reducing the temperature of each polymer–TDF–D_2O solution to below the hydrate dissociation temperature, it was found that the conformation of PEO does not change on hydrate formation, with no evidence of an adsorbed layer. Conversely, PVP showed an increase in the low q-scattering amplitude in comparison to PEO on hydrate formation and a higher level of scattering at the higher q-values was also observed. PVCap and VIMA/VCap were found to exhibit even larger low q-scattering amplitudes than PVP and were also adsorbed on the hydrate surface.

If there was no interaction between the polymer and the hydrate surface, the data could be modelled using a linear combination of polymer solution scattering and Porod scattering which is from the crystal–liquid interface in a partially frozen sample (Porod scattering gives an indication of the surface area present). However, the data could not be modelled in this way, and therefore it was suggested that PVP, PVCap and VIMA/VCap are adsorbed onto the hydrate surface, further indicating the mode of action of these polymer inhibitors. Conversely, by including a term to account for scattering from the polymer adsorbed onto the hydrate crystals, the authors were able to describe the total scattering for these systems.[47] The higher amplitudes of the low-q scattering along the series PEO < PVP < PVCap, VIMA/VCap were attributed to greater surface coverage by the inhibitor, which interestingly also corresponds to the increasing effectiveness of the polymers as hydrate inhibitors.[47]

4 Hydrate decomposition

4.1 Controlled decomposition

Controlled decomposition studies have been performed by Stern *et al.* on pure, polycrystalline methane hydrate (CH_4·5.89H_2O) at 1 atm over the temperature range 193 to 290 K.[48] The volume of gas released during the experiments was measured using a gas flow meter (*cf.* a Torricelli tube). The methane hydrate dissociation process was found to depend upon

the procedure used to destabilize the hydrate. Using a temperature-ramping procedure, decomposition was reproducible with 97% of methane within the hydrate lattice being released over the temperature range 198 to 220 K. From 220 to 260 K, less than 1% further decomposition occurred, and above 260 K the remaining 2% of methane gas from the hydrate sample was released.

Using a pressure-release procedure to destabilise the hydrate samples, monotonic dissociation was observed over the temperature range 195 to 220 K, with dissociation rates increasing with temperature (*cf.* the dissociation behaviour for temperature-ramping measurements over this temperature range). The time-scales of decomposition (>85% dissociation) were approximately 5 hours and 7 minutes at dissociation temperatures of 204 and 239 K, respectively. In contrast, rapid depressurisation to 1 atm over the temperature range 242 to 271 K revealed anomalous decomposition behaviour compared to the previously observed monotonic behaviour. This anomalous behaviour consists of a short rapid dissociation phase with a release of 5–20 vol% of the total methane in the hydrate sample. During this gas release, adiabatic cooling of methane as well as general heat absorption occur, resulting in a drop in temperature of between 3 and 7 K relative to the temperature of the external cooling bath. After this rapid dissociation phase, the methane hydrate remains 'metastably preserved' for up to 24 hours. Stern *et al*. also found that carbon dioxide hydrate could be 'preserved' under similar conditions.[48] X-Ray diffraction studies confirmed that the preserved methane hydrate material consists of sI hydrate, although visual observations indicated that the preserved material has a different texture to that of as-synthesized methane hydrate.[48] The former is less prone to fracturing or flaking during cleaving and is less granular in appearance. These findings are believed to be potentially significant with regard to the exploitation of natural gas hydrate marine sediments and may offer a strategy for retrieving these deposits in a safe and controlled manner.

4.2 Gas hydrates in porous media

Equilibrium pressures for gas hydrate formation in ocean sediments are thought to be dependent on capillary forces between the solid phase and liquid water within the pores of the sediments. Handa and Stupin[49] showed that the dissociation pressures of methane and propane hydrates formed in silica gel (with a nominal pore radius of 7.5 nm) are higher than those measured from the bulk phases. Similarly, Uchida *et al*.[50] showed that for methane hydrate formed in porous silica glass (Vycor glass with average pore diameters of 11.9 to 49.5 nm), the dissociation temperature is lower and the dissociation pressure is higher than for bulk methane hydrate. Uchida *et al*.[50] attributed this shift in dissociation conditions of methane hydrate in these small pores to the changes in the activity of the water molecules and estimated the apparent free energy between methane hydrates and water in the confined geometry to be about 3.9×10^{-2} J m^{-2} (*cf.* that between ice and water in similar porous media).

Clarke *et al*.[51] have developed a predictive method that incorporates the properties of porous media with the van der Waals and Platteeuw model to give the equilibrium relationship for hydrate formation in porous media. Considering hydrate formation in porous media being analogous to the behaviour of a fluid in a capillary, the following properties of porous media have been incorporated into this predictive method: the surface tension, the wetting angle (the angle between the capillary wall and the meniscus), and the pore radius. Klauda and Sandler[52] have also developed a hydrate phase equilibrium model to predict hydrate formation in porous media. This model is based on a fugacity approach and extends the van der Waals and Platteeuw approach.[20] Unlike the method developed by Clarke *et al*.,[51] which only considers a single pore size, this model takes into account the distribution of pore sizes in porous media.

The model[52] is based on the following considerations: freezing of water in pores is believed to proceed from large pores to small pores (such that at equilibrium there is a distribution of pores containing frozen water and pores containing liquid water); the interface between solid and liquid phases is important within a pore (in particular, the fugacity of liquid water in the pore is affected by surface tension across the hydrate–liquid water interface). Therefore, the pore size distribution of the sediments and the surface tension between the hydrate and liquid water have been incorporated into this model.

Calculations of the L–H–V phase equilibria (where L = liquid water, H = hydrate, V = hydrate former vapour) in porous media using this model[52] and that of Clarke *et al*.[51] were found to give reasonably good agreement with experimental data.[49] However, phase equilibria predictions in porous media at temperatures below the normal freezing point of water were found to be less accurate than calculations performed above the freezing point. These discrepancies suggest the need for experimental studies on the H–I–L (where I = ice) interface in porous systems for better predictions of the equilibrium pressures.

5 Future prospects

Although the thermodynamic and phase equilibria properties of gas hydrates have been extensively studied over the last decade or so, it is clear that the solution to controlling gas hydrate formation for gas exploration, transportation and production will require further measurements of this type. These measurements should be coupled with structural phase equilibria measurements, using techniques such as Raman and NMR spectroscopies and X-ray and neutron diffraction. In addition, although there have been some key kinetic studies using both macroscopic and microscopic tools, this area of hydrate research needs to be further explored to provide further detailed kinetic data on hydrate formation, inhibition and decomposition. In particular, it has been demonstrated that *in situ* time-resolved techniques such as Raman spectroscopy, X-ray and neutron diffraction are extremely powerful probes for providing a fundamental understanding of gas hydrate formation and decomposition. Knowledge of the kinetics and mechanisms of gas hydrate crystal growth and decomposition will have wide reaching implications concerning a range of applied issues, including the safe and efficient exploitation of gas hydrate marine sediments, understanding the role of gas hydrates in space, in comets, and in glaciological contexts, and controlling gas hydrates in gas and oil pipelines. In particular, the optimal design of effective chemicals for gas hydrate control will undoubtedly depend upon obtaining both quantitative hydrate formation/decomposition measurements and mechanistic information from macroscopic and structural studies, in addition to empirical measurements. Furthermore, a fundamental understanding of the properties of gas hydrates will be important for inclusion chemistry[53] in general.

6 Acknowledgements

I would like to thank my earlier and present co-workers at King's College London, the ISIS facility at the Rutherford Appleton Laboratory, and the Daresbury Laboratory. Financial support from the Gas Research Institute, Chevron Petroleum

Research, DeepStar Industry Consortium, NATO, and EPSRC is gratefully acknowledged.

7 References

1 H. Davy, *Philos. Trans. R. Soc. London*, 1811, **101**, 1–35.
2 M. Faraday, *Philos. Trans. R. Soc. London*, 1823, **113**, 160–165.
3 E. D. Sloan, *Clathrate Hydrates of Natural Gases*, 2nd Edition, Marcel Dekker, NY, 1997.
4 K. A. Udachin, C. I. Ratcliffe and J. A. Ripmeester, *Angew. Chem., Int. Ed.*, 2001, **40**, 1303–1305.
5 R. K. McMullan and G. A. Jeffrey, *J. Chem. Phys.*, 1965, **42**, 2725–2732.
6 K. T. Mak and R. K. McMullan, *J. Chem. Phys.*, 1965, **42**, 2732–2737.
7 J. A. Ripmeester, J. S. Tse, C. I. Ratcliffe and B. M. Powell, *Nature*, 1987, **325**, 135–136; K. A. Udachin, C. I. Ratcliffe, G. D. Enright and J. A. Ripmeester, *Supramol. Chem.*, 1997, **8**, 173–176.
8 J. C. Landry and A. W. England, *Geophys. Res. Lett.*, 1994, **21**, 2829–2832.
9 J. S. Loveday, R. J. Nelmes, M. Guthrie, S. A. Belmonte, D. R. Allan, D. D. Klug, J. S. Tse and Y. P. Handa, *Nature*, 2001, **410**, 661–663.
10 M. Chou, A. Sharma, R. C. Burress, J. Shu, M. Ho-kwang, J. Hemley, A. F. Goncharov, L. A. Stern and S. H. Kirby, *Proc. Natl. Acad. Sci. U. S. A.*, 2000, **97**, 13484–13487.
11 P. Englezos, *Ind. Eng. Chem. Res.*, 1993, **32**, 1251–1274.
12 C. A. Koh, R. E. Westacott, W. Zhang, K. Hirachand, J. L. Creek and A. K. Soper, *Fluid Phase Equilib.*, 2002, **194–197**, 143–151.
13 K. Kvenvolden, *Rev. Geophys.*, 1993, **31**, 173–187.
14 T. S. Collett and M. W. Lee, *Ann. N. Y. Acad. Sci.*, 2000, **912**, 51–64.
15 C. R. Fisher, I. R. MacDonald, R. Sassen, C. M. Young, S. A. Macko, S. Hourdez, R. S. Carney, S. Joye and E. McMullin, *Naturwissenschaften*, 2000, **87**, 184–187.
16 G. J. MacDonald, *Clim. Change*, 1990, **16**, 247–281.
17 S.-P. Kang and H. Lee, *Environ. Sci. Technol.*, 2000, **34**, 4397–4400.
18 E. D. Sloan, *Ind. Eng. Chem. Res.*, 2000, **39**, 3123–3129.
19 J. P. Lederhos, J. P. Long, A. Sum, R. L. Christiansen and E. D. Sloan, *Chem. Eng. Sci.*, 1996, **51**, 1221–1229.
20 J. H. van der Waals and J. C. Platteeuw, *Adv. Chem. Phys.*, 1959, **2**, 1–57.
21 W. R. Parrish and J. M. Prausnitz, *Ind. Eng. Chem. Proc. Des. Dev.*, 1972, **11**, 26–34.
22 G. D. Holder and G. C. Grigoriou, *J. Chem. Thermodyn.*, 1980, **12**, 1093–1104.
23 J. B. Klauda and S. I. Sandler, *Ind. Eng. Chem. Res.*, 2000, **39**, 3377–3386.
24 R. E. Westacott and M. P. Rodger, *Chem. Phys. Lett.*, 1996, **262**, 47–51.
25 S. R. Zele, S.-Y. Lee and G. D. Holder, *J. Phys. Chem. B*, 1999, **103**, 10250–10257.
26 S. Subramanian, R. A. Kini, S. F. Dec and E. D. Sloan, *Chem. Eng. Sci.*, 2000, **55**, 1981–1999.
27 J. A. Ripmeester, C. I. Ratcliffe, D. D. Klug and T. S. Tse, *Ann. N. Y. Acad. Sci.*, 1994, **715**, 161–176.
28 A. K. Sum, R. C. Burruss and E. D. Sloan, *J. Phys. Chem. B*, 1997, **101**, 7371–7377.
29 K. Morita, S. Nakano and K. Ohgaki, *Fluid Phase Equilib.*, 2000, **169**, 167–175.
30 M. Bach-Verges, S. J. Kitchin, K. D. M. Harris, M. Zugic and C. A. Koh, *J. Phys. Chem. B*, 2001, **105**, 2699–2706.
31 P. Servio, P. Englezos and P. R. Bishnoi, *Ann. N. Y. Acad. Sci.*, 2000, **912**, 576–582.
32 P. Englezos, N. Kalogerakis, D. Dholabhai and P. R. Bishnoi, *Chem. Eng. Sci.*, 1987, **42**, 2647–2658.
33 E. D. Sloan, S. Subramanian, P. N. Matthews, J. P. Lederhos and A. A. Khokhar, *Ind. Eng. Chem. Res.*, 1998, **37**, 3124–3132.
34 C. A. Koh, J. L. Savidge and C. C. Tang, *J. Phys. Chem.*, 1996, **100**, 6412–6414.
35 K. A. Udachin, C. I. Ratcliffe and J. A. Ripmeester, *J. Phys. Chem. B*, 2001, **105**, 4200–4204.
36 R. W. Henning, A. J. Schultz, V. Thieu and Y. Halpern, *J. Phys. Chem. A*, 2000, **104**, 5066–5071.
37 L. A. Stern, D. L. Hogenboon, W. B. Durham, S. H. Kirby and I.-M. Chou, *J. Phys. Chem. B*, 1998, **102**, 2627–2632.
38 C. A. Koh, R. E. Westacott, R. P. Wisbey, X. Wu and A. K. Soper, *J. Chem. Phys.*, 2000, **113**, 6390–6397.
39 D. T. Bowron, A. Filipponi, M. A. Roberts and J. L. Finney, *Phys. Rev. Lett.*, 1998, **81**, 4164–4167.
40 P. Clancy and L. Baez, *Ann. N. Y. Acad. Sci.*, 1994, **715**, 177–186.
41 R. E. Westacott and P. M. Rodger, *J. Chem. Soc., Faraday Trans.*, 1998, **94**, 3421–3426.
42 J. S. Tse, V. P. Shpakov, V. V. Murashov and V. R. Belosludov, *J. Chem. Phys.*, 1997, **107**, 9271–9274.
43 H. Tanaka, Y. Tamai and K. Koga, *J. Phys. Chem. B*, 1997, **101**, 6560–6565.
44 J. M. Cohen, P. F. Wolf and W. D. Young, *Energy Fuels*, 1998, **12**, 216–218.
45 T. J. Carver, M. G. B. Drew and P. M. Rodger, *J. Chem. Soc., Faraday Trans.*, 1995, **91**, 3449–3460.
46 R. Larsen, C. A. Knight and E. D. Sloan, *Fluid Phase Equilib.*, 1998, **150–151**, 353–360.
47 H. E. King, J. L. Hutter, M. Y. Lin and T. Sun, *J. Chem. Phys.*, 2000, **112**, 2523–2532.
48 L. A. Stern, S. Circone, S. H. Kirby and W. B. Durham, *J. Phys. Chem. B*, 2001, **105**, 1756–1762.
49 Y. P. Handa and D. Stupin, *J. Phys. Chem.*, 1992, **96**, 8599–8603.
50 T. Uchida, T. Ebinuma and T. Ishizaki, *J. Phys. Chem. B*, 1999, **103**, 3659–3662.
51 M. A. Clarke, M. Pooladi-Darvish and P. R. Bishnoi, *Ind. Eng. Chem. Res.*, 1999, **38**, 2485–2490.
52 J. B. Klauda and S. I. Sandler, *Ind. Eng. Chem. Res.*, 2001, **40**, 4197–4208.
53 K. D. M. Harris, *Chem. Br.*, 1993, **29**, 132–136.